JOURNAL OF GEOPHYSICAL RESEARCH, VOL. 105, NO. B3, PAGES 5663–5677, MARCH 10, 2000

A convection model to explain anisotropy of the inner core

H.-R. Wenk,[1] J. R. Baumgardner,[2] R. A. Lebensohn,[3] and C. N. Tomé[4]

Abstract. Seismic evidence suggests that the solid inner core of the Earth may be anisotropic. Several models have been proposed to explain this anisotropy as the result of preferred orientation of crystals. They range from a large annealed single crystal, growth at the melt interface, to deformation-induced texture. In this study texture development by deformation during inner core convection is explored for ε-iron (hcp) and γ-iron (fcc). Convection patterns for harmonic degree two were investigated in detail. In the model it is assumed that traces of potassium are uniformly dispersed in the inner core and act as a heat source. Both for fcc and hcp iron, crystal rotations associated with intracrystalline slip during deformation can plausibly explain a 1-3% anisotropy in *P* waves with faster velocities along the N-S axis and slower ones in the equatorial plane. The effect of single crystal elastic constants is explored.

1. Introduction

The nature, composition, and structure of the solid inner core of the Earth has fascinated geophysicists for many years [e.g., *Anderson,* 1980; *Jeanloz,* 1990; *Stevenson,* 1981]. Ever since the discovery of seismic anisotropy in the inner core [*Morelli et al.,* 1986; *Woodhouse et al.,* 1986], the implications for its structure have been discussed. There is still a lot of controversy and rarely a subject has received so much attention in prestigious journals such as *Science* and *Nature*. Some remain convinced that it exists [e.g., *Song,* 1997]; others are doubtful [*Bréger et al.,* 1999]. Some think that it is confined to the outer layer [*Tromp,* 1993]; others believe that anisotropy is closer to the center [*Song and Helmberger,* 1995]. Elastic constants are claimed to be highly anisotropic [*Mao et al.,* 1998]; others think that they are close to isotropic [*Stixrude and Cohen,* 1995]. The inner core may rapidly rotate relative to the mantle [*Song and Richards,* 1996] or not rotate at all [*Buffett and Creager,* 1998]. Proposals for crystal alignment in the inner core range from deformation-induced texturing during convection [*Jeanloz and Wenk,* 1988; *Wenk et al.,* 1988], growth in a stress field [*Yoshida et al.,* 1996], growth in a magnetic field [*Karato,* 1993], deformation in a magnetic field [*Karato,* 1999], solidification texturing at the boundary with the liquid outer core [*Bergman,* 1997] to a gigantic single crystal, 2500 km in diameter, growing in a melt [*Stixrude and Cohen,* 1995]. Such a crystal would be about 5 orders of magnitude larger than the largest crystal presently known and is difficult to imagine. The controversy clearly illustrates how little we really know about the inner core. In fact, in spite of many detailed studies and a large literature, there is still uncertainty about the phase composition of the inner core, the melting temperature, and there is no agreement about the distribution of anisotropy, not to speak of the mechanisms that produce it. In this report we add a piece to this puzzle by combining new methods of materials science, mechanics, and geodynamics to revisit core convection. We do not exclude any of the hypotheses but simply investigate, on a quantitative level, how anisotropy could plausibly develop if certain conditions prevail.

Many seismologic studies have confirmed the original observations [*Morelli et al.,* 1986; *Woodhouse et al.,* 1986] that compressional waves travel 3 to 4% faster along the (vertical) axis of the Earth, than in the equatorial plane [e.g. *Creager,* 1992; *Romanowicz et al.,* 1996; *Shearer et al.,* 1988; *Shearer,* 1994; *Song and Helmberger,* 1995; *Su and Dziewonski,* 1995; *Tromp,* 1993; *Vinnik et al.,* 1994], though a recent study suggests that this conclusion may be an artifact due to heterogeneities in the core-mantle boundary [*Bréger et al.,* 1999] and the picture is clearly more complicated. In this study we assume that anisotropy exists and are exploring a possible mechanism by which it developed.

A directional dependence of seismic wave propagation speed can either be due to a layered structure with components of highly contrasting elastic properties (e.g., solid-liquid, solid with oriented open fractures) or due to an alignment of crystals with anisotropic elastic properties (texture). The former is an important consideration for sediments at the Earth's surface [*Crampin,* 1981] but highly unlikely at the high pressure and temperature of the inner core.

There are various ways in which a preferred alignment of crystals can originate. It can either be a result of primary growth (examples are fibrous growth of quartz on a flat surface, epitaxial growth of a superconducting oxide on a single crystal substrate or growth in a melt with a temperature gradient [*DeRango*

[1]Department of Geology and Geophysics, University of California, Berkeley.
[2]Theoretical Division,Los Alamos National Laboratory, Los Alamos, New Mexico.
[3]CONICET (Consejo Nacional de Investigaciones Cientificas y Técnicas), University of Rosario, Rosario, Argentina.
[4]Materials Science and Technology Division, Los Alamos National Laboratory, Los Alamos, New Mexico.

Paper number 1999JB900346.
0148-0227/00/1999JB900346$09.00

et al., 1991; *Huang et al.*, 1985; *Selvamanickam and Salama,* 1990]), of deformation by dislocation glide (as in cold-worked metals or tectonically deformed rocks), or of secondary growth of a deformed aggregate by recrystallization (minerals in many recrystallized metamorphic rocks show preferred orientation patterns). The preferred orientation (or texture) that develops during recrystallization is related to the deformation texture [e.g., *Doherty,* 1997; *Haessner,* 1978; *Humphreys and Hatherly,* 1995; *Wenk et al.,* 1997].

Deformation in the Earth's interior is pervasive. It is generally accepted that convection occurs in the solid mantle and in the liquid core. Models of mantle convection with finite element methods and polycrystal plasticity theory have confirmed that strong and locally heterogeneous textures (FEM) are produced that result in characteristic seismic anisotropy [*Chastel et al.,* 1993, *Dawson and Wenk,* 1999]. In this paper we follow up on the intuitive suggestion of *Jeanloz and Wenk* [1988] that convection may also exist in the solid inner core, and formulate a quantitative model, exploring the limitations and possibilities of such a mechanism for the development of seismic anisotropy. We will show that, with realistic assumptions about geometry, composition, boundary conditions, and mechanisms, convection in a sphere with an internal heat source does indeed produce strong crystallite alignment, sufficient to explain the observed seismic anisotropy. We will also show that the intuitive conclusions of *Jeanloz and Wenk* [1988] about crystal alignment during convection were wrong.

The model that we present is simplified to explore general features rather than detailed local structures. Contrary to the mantle, where the case for convection is very straightforward, many parameters for the core are much less defined, and the spherical geometry introduces considerable numerical complications.

2. Finite Element Model of Core Deformation

Estimates for the physical parameters used to model inner core convection are listed in Table 1. Most of the values in this table are constrained to within 10% by seismological observations, by high-pressure mineral physics experiments, or by a combination of the two. Larger uncertainties, however, are associated with the radiogenic heating rate, the dynamic viscosity, and perhaps also the thermal conductivity. But only the uncertainty in the radiogenic heating impacts the results in any significant way, as discussed below.

Convection is pervasive in the liquid outer core [e.g., *Glatzmaier and Roberts,* 1995, 1996]. However, before attempting to explain anisotropy in the inner core as a result of convection, it needs to be established whether convection can occur at all. A basic requirement in this regard is that the heat production be large enough to sustain a superadiabatic temperature gradient, at least near the inner core surface. We can obtain a minimum value for the required heat production rate from Fourier's law for conductive heat transfer, $q = k\, dT/dz$, together with the relation for the adiabatic gradient, $dT_{adb}/dz = \alpha g T/c_p$. Here q is heat flux per unit area, k is thermal conductivity, T is absolute temperature, z is depth, α is the volume coefficient of thermal expansion, g is gravitational acceleration, and c_p is specific heat at constant pressure. If we assume uniform volumetric heating, the minimum heat production H_{min}, required to sustain an adiabatic condition, is given by $H_{min} = 3k\alpha g T/r_0 c_p$, where r_0 is the inner core radius. The parameters in Table 1 yield a value for H_{min} of 4×10^{-8} W/m^3 and corresponds to a total heat production in the inner core of 3×10^{11} W. This value for H_{min} is a factor of 40 larger than the value from *Merrill and McElhinny* [1983, Table 1]. Therefore it seems at first that convection is unlikely.

There are at least two conceivable sources for heating of the inner core. Uranium and thorium contribute of the order of 2.3×10^{13} W to the current heat generation budget for the Earth [*Stacey,* 1992]. If about 1% of the Earth's U and Th were originally concentrated in the core and gravitationally segregated at its center before inner core freezing began, it would provide sufficient heat to drive inner core convection.

Similarly, if a modest fraction, of the order of 2-10%, of the planetary potassium were initially segregated into the core and concentrated in the solid phase, the resulting heat production would suffice [*Jeanloz,* 1990]. Compared to chondritic composition, the crust and upper mantle are deficient in K. A concentration of K in the core also seems to be justified because at high pressures an electronic phase transition in potassium compresses its 4*s* valence electrons into the empty 3*d* shells and potassium attains a siderophile character. Potassium, at lower mantle and core pressures, behaves as a first transition series metal like iron and nickel [*Bukowinski,* 1976, 1979] and is likely to form alloys with iron [*Parker et al.,* 1996] and exist in the solid inner core.

The three-dimensional spherical finite element code TERRA [*Baumgardner,* 1985, 1988] is applied to

Table 1. Inner Core Parameters

Parameter	Value	Reference
Mean density, kg m^{-3}	12,850	*Masters and Shearer* [1990]
Radius, 10^6 m	1.22	*Masters and Shearer* [1990]
Surface temperature, K	5500	*Stixrude and Brown* [1998]
Specific heat, J kg^{-1} K^{-1}	840	*Glatzmaier and Roberts* [1996]
Heat production, W m^{-3}	10^{-9}	*Merrill and McElhinny* [1983]
Thermal expansion, K^{-1}	10^{-5}	*Glatzmaier and Roberts* [1996]
Thermal conductivity, W m^{-1} K^{-1}	60	*Stixrude and Brown* [1998]
Dynamic viscosity, Pa s	$10^{16(+/-3)}$	*Frost and Ashby* [1982]

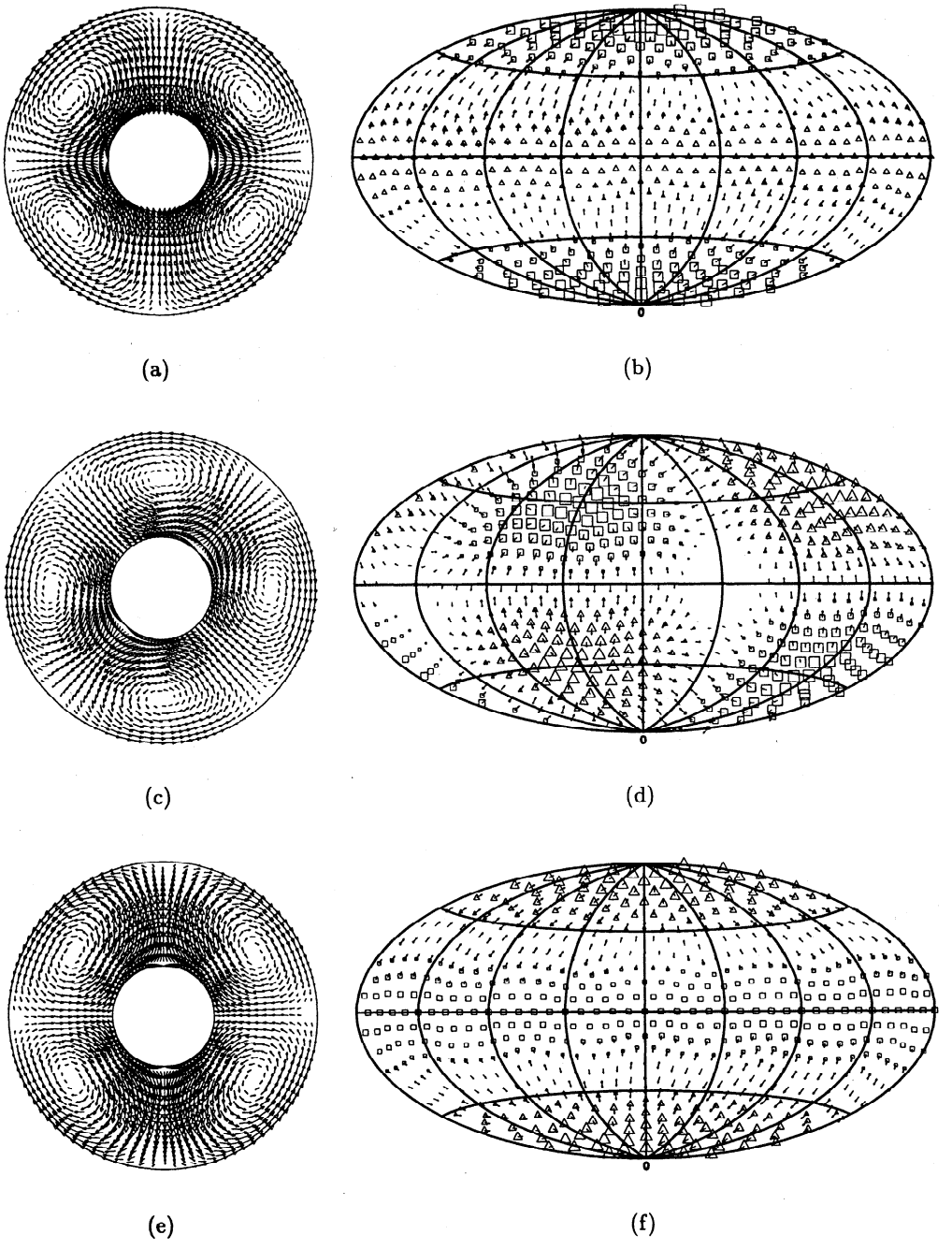

Figure 1. (a-c) Cross sections and (d-f) surface images at middepth of the velocity field for three different mostly degree two harmonic patterns that alternate in time during internally heated convection in the inner core. Triangles denote radial upward flow, and squares denote radially downward flow. Peak velocities are approximately 10 cm/y in all cases.

model the problem of inner core convection. Since TERRA is designed to address spherical shell geometries, we treat the inner core as a spherical shell rather than a complete sphere because convection through the center of the sphere would introduce singularities. A small rigid sphere with a radius of 400 km (representing 0.15% of the volume of the core as a whole and 3.5% of the volume of the inner core) is introduced. We have shown with numerous simulations that such a small rigid sphere in the center has a minimum influence on the flow pattern. While this geometry was chosen for numerical reasons and is arbitrary, it may have a physical justification if insoluble elements heavier than iron concentrate in the center of the core. The geometry implies a harmonic degree two convection pattern will be favored, based on analytical marginal stability considerations as well as prior numerical investigations at supercritical Rayleigh numbers [*Chandrasekhar,* 1961, *Zebib et al.,* 1983], and the results will be shown for that case.

The outer boundary (with the liquid outer core) is taken to be isothermal and free slip, with a fixed

temperature of 5500 K. We choose an insulating boundary condition for the inner boundary, which implies 100% internal heating for the shell. For computational reasons we choose a free slip stress condition also for this boundary. We assume an adiabatic reference temperature for the shell and use a linear equation of state to obtain density differences from deviations in temperature relative to the adiabatic reference state. The material is assumed to be a Newtonian fluid. We assume a heating rate only 0.001 times larger than that required to maintain an adiabatic temperature profile near the top of the inner core. This yields a Rayleigh number of approximately 100 times the critical value, using the parameters from Table 1, including a dynamic viscosity of 1 x 10^{16} Pa s.

As an initial temperature distribution we choose a degree two spherical harmonic perturbation to the adiabatic reference state with positive values of temperature perturbation around the equator. Although this solution appears stable for a few convective overturns, at longer times the pattern is found to alternate among three degree two patterns and never attain a steady state. The three patterns include one with upwelling along a great circle and downwelling centered at the two points 90° away (north and south poles) (M=2, L=0); one with downwelling along a great circle and upwelling centered at the two points 90° away (north and south poles); and one with two zones of upwelling and two zones of downwelling, alternating around a great circle (M=2, L=2). The velocity distribution for these three stages is illustrated in Figures 1a-1f. The first of these three patterns seems to be preferred in a time-average sense over the other two and is chosen for computing the development of texture and anisotropy in this paper. A cross section with three streamlines is illustrated in Figure 2. The numerical calculations suggest convection in the inner core may not be steady over very long time spans and that the pattern we are selecting may not correspond to exactly the one which currently exists. Nevertheless, we believe the pattern and magnitude of anisotropy it generates is illustrative of the manner convection processes can operate in the inner core.

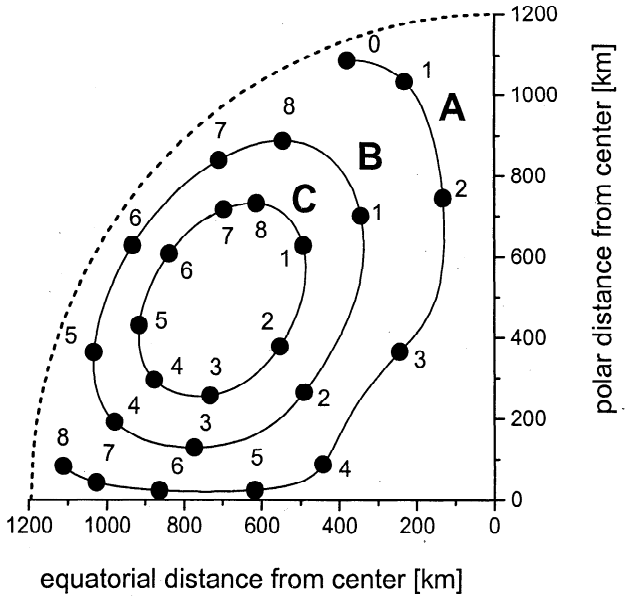

Figure 2. Streamlines for degree two harmonic convection during stage in Figure 1a with axial symmetry, subduction at poles, and extrusion in the equatorial plane. Three streamlines, A, B, and C are indicated, with eight positions for which textures were evaluated. For positions 1, 3, 5, and 7 of outer streamline (A) and intermediate streamline (B) textures are displayed in Figures 6 and 7 and discussed in the text.

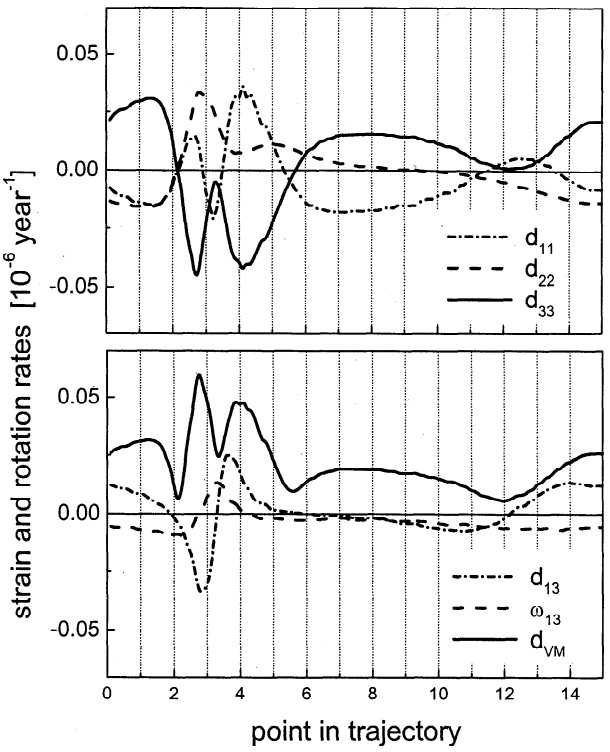

Figure 3. Strain rate components for external streamline A in Figure 2, expressed in equatorial/polar reference system.

As far as the FEM model is concerned, the material is chosen as an isotropic medium. This is different from the approach used in modeling anisotropy development in the upper mantle [*Chastel et al.,* 1993; *Dawson and Wenk,* 1999] where the medium was anisotropic and each element representative of an assembly of crystals. In those studies it was observed that the anisotropy did not have a major influence on the flow pattern, and given the large uncertainties in the inner core and the exploratory character of this investigation, an isotropic approach seemed justified.

The deformation at a certain time increment was evaluated along selected streamlines. In all cases we observe large strains along streamlines and correspondingly expect strong texture development. The strain evolution along a streamline is rather complicated. Figure 3 shows cyclic changes in some components of the symmetric and skewsymmetric parts of the strain rate tensor calculated for the outer streamline in Figure 2 (labeled A), starting near the north-pole (at point 0). At the beginning, the strain state

consists mainly in extension along x_3 (N-S) direction (i.e., large positive d_{33}) but this is reversed after point 2 to become compressive along this direction (negative d_{33}). The components d_{11} and d_{22} are complementary to d_{33}. During spreading (from point 6 to 14) the material mainly undergoes a plain strain deformation (extension along N-S and shortening along E-W). At those points, the diagonal components as well as the shear strain rate d_{13} are minimal and no further texture evolution takes place, only a rigid rotation of the pre-existent texture. Correspondingly, the Von Mises equivalent strain rate d_{VM} is also relatively low during spreading and large during downwelling and extrusion. The spin rate component ω_{13}, which gives the rigid body rotation relative to the Cartesian reference frame, also reaches a maximum during subduction-extrusion and a minimum during spreading. Furthermore, whereas the sign of ω_{13} practically does not change throughout the trajectory (except for a short interval near point 5) the representative material rotates almost always in the same sense, making a complete turn after one cycle.

3. Polycrystal Plasticity

From these FEM simulations it is evident that if convection occurs, deformations are large and the deformation path is rather complex. If the material is polycrystalline it has to conform to laws of polycrystal plasticity. Depending on material characteristics and conditions, deformation may occur by volume or grain boundary diffusion or by dislocation movements. With decreasing stress, diffusion mechanisms gain in importance. We assume that deformation by slip produces lattice reorientations. Additional climb and recovery would weaken texture evolution, and dynamic recrystallization may modify the orientation pattern [*Humphreys and Hatherly,* 1995]. These mechanisms are difficult to model in the absence of experimental data for ε-iron. By analogy to other materials we do not expect a major influence on anisotropy development [e.g., *Wenk and Tomé,* 1999].

The complex mutual influence of anisotropy, lattice preferred orientation, and plastic deformation of real polycrystalline materials has been a matter of extensive research [e.g., *Kocks et al.,* 1998]. A real polycrystal deforms maintaining local stress equilibrium and strain compatibility. This is achieved through the development of intergranular and intragranular heterogeneities (i.e., variation of stress and strain from grain to grain and within grains, respectively). Such a situation is extremely difficult to model and therefore some simplifications are necessary. The "upper bound" *Taylor* [1938] model which assumes homogeneous deformation throughout the polycrystal, regardless of crystal orientation, and the "lower bound" *Sachs* [1928] model which assumes stress equilibrium and sacrifices strain compatibility are among the simplest polycrystal models that have been applied to simulate deformation by intracrystalline slip.

Unlike Taylor or Sachs approaches, which assume that strain rate or stress is the same in all grains, respectively, a viscoplastic self-consistent (VPSC) formulation [*Molinari et al.,* 1987] provides more freedom for grains to deform individually, depending on orientation. The VPSC model basically regards each grain of the polycrystal as a viscoplastic inclusion deforming in a viscoplastic homogeneous but anisotropic effective medium having the average properties of the polycrystal. The VPSC model, in its 1-site [*Lebensohn and Tomé,* 1993] and *n*-site [*Canova et al.,* 1992] approximations, has been widely used for the prediction of deformation textures in metals and minerals [*Tomé and Canova,* 1998; *Wenk,* 1999].

A polycrystal plasticity model requires as input knowledge about the crystallography of the phases which are present, the active intracrystalline deformation mechanisms such as slip and mechanical twinning, including critical resolved shear stresses for slip systems and their strain rate sensitivity (often expressed as stress exponent). The initial crystallographic and morphologic orientation distributions of the constituent grains are also required. The simulation then consists in imposing a deformation history in incremental steps of strain. In the case presented here we use the strain evolution along a streamline as predicted by the finite element model. As a strain is imposed to all grains, the material responds with an average stress. In each grain, slip systems are activated and the shear on each system is recorded. This shear may cause hardening of the critical shear stresses. Since the materials under consideration is close to the melting point, significant hardening is unlikely and was omitted.

Also the grain morphology may change along the simulation. Due to plastic deformation, the ellipsoids representing the grains may rotate and become elongated in some directions and flat in others. However, for the core's conditions of high temperature and low strain rate, it is plausible to assume that diffusion mechanisms will prevent any morphologic evolution and therefore the grains will remain equiaxed throughout the deformation process.

As plastic deformation occurs, there is a lattice rotation of the crystal relative to its orientation in the previous step. This rotation can be described as the superposition in terms of three different components: a macroscopic spin, a local spin, and a plastic spin [*Lebensohn and Tomé, 1993*]. The first one (macro) is given by the overall rotation of the polycrystal (skew-symmetric part of the average displacement gradient). The second one (local) depends on the magnitude of the local deviations in strain with respect to the average and on the assumed grain shape. The third component (plastic) can be derived from the shears on the slip systems. Particularly, the local component vanishes for spherical grains, which is the case in this calculation.

Due to these rotations, a new orientation distribution evolves, and this is of primary interest in the present paper. Since physical properties of an aggregate are related to the properties of single crystals, we can simulate the evolution of macroscopic physical properties from knowledge of crystal orientations

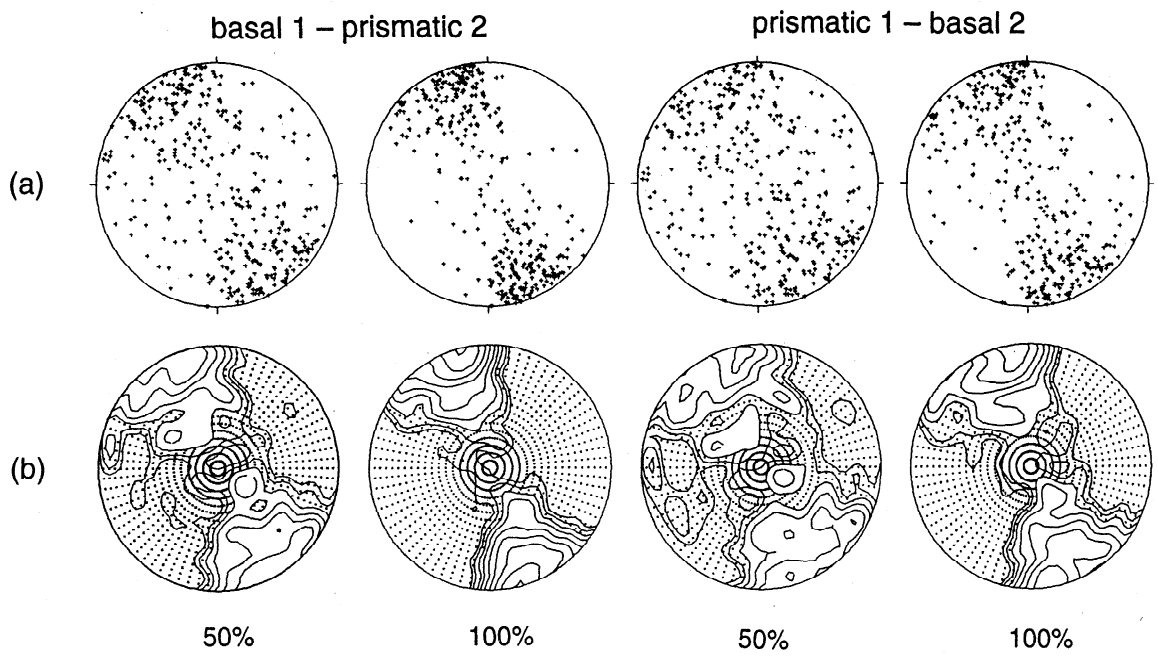

Figure 4. Simulation of texture development for a hexagonal metal deformed in simple shear to a strain of 50% and 100%. (a) Pole figures with discrete *c* axes (0001). (b) Pole densities are contoured and expressed in multiples of a random distribution; logarithmic contours, dot pattern below 1 multiples of a random distribution (m.r.d.). The figure compares results for different critical shear stresses. (left) Basal slip is twice as easy as prismatic slip; (right) Basal slip is twice as hard as prismatic slip. Projection is equal area; macroscopic shear plane and shear direction are indicated.

averaged over appropriate volumes. In the case of a convection cell there is heterogeneity of crystal orientations on two scales.

First, there is heterogeneity within the convection cell depending on the location of the material within the cell. In order to obtain average elastic properties of the inner core, one has to average over textures in all locations, giving proper weight to the volume that each represents.

Second, there is also heterogeneity on the scale of an aggregate. An orientation distribution may be random or non random. This is most easily represented in pole figures that illustrate the distribution of a particular crystallographic direction, projected on a sphere. Figure 4 shows *c* axis (0001) pole figures for deformation simulations of a hexagonal metal in simple shear. The shear plane is horizontal. In Figure 4a (top) the texture is represented with (0001) poles, each corresponding to a crystal. A continuous distribution can be obtained, for example, by fitting each orientation with a Gaussian and contouring on the sphere locations of equal orientation density (for representations and data transformations the software BEARTEX was used [*Wenk et al.,* 1998]). Generally, pole densities are compared with those of an aggregate with a random orientation distribution as illustrated for the same textures in Figure 4b (bottom).

As mentioned above, a central ingredient to polycrystal plasticity is the identity of the phase and the active slip systems. The phase diagram of iron at high pressure and high temperature has been investigated experimentally and theoretically, but there is still considerable debate about phase relations in the inner core. There is general agreement that the main component is an iron-rich alloy, but there is uncertainty about how pure this Fe-Ni alloy is [e.g., *Mao et al.,* 1990], and there are suggestions that sulfides may be present [*Jephcoat and Olson,* 1987; *Anderson and Ahrens,* 1996]. From shock experiments the melting curve has been determined, and this puts constraints on the boundary between the liquid outer core and the solid inner core [e.g., *Anderson,* 1990; *Boehler,* 1993; *Williams et al.,* 1987]. It has been established that the most likely phases are either hexagonal close-packed (ε-iron, hcp), or cubic close-packed (γ-iron, fcc) (e.g., experiments by *Brown and McQueen*[1986], *Jephcoat et al.*[1986], *Yoo et al.* [1995], *Mao et al.*[1998], and first principles calculations by *Singh et al.*[1991], *Soderlind et al.*[1996], *Stixrude and Cohen*[1995], *Wasserman et al.*[1996]). Some experimental studies suggest that yet other polymorphs of iron, related to the hexagonal structure, may be present [*Sayers,* 1990; *Ross et al.,* 1990; *Saxena et al.,* 1993]. In this study we investigate only fcc and hcp iron, and the specific results apply to these two crystal structures, but general conclusions about polycrystal plasticity and texture development would be valid for other phases as well.

As far as slip systems are concerned, the case is straightforward for fcc where the slip mode {111}<110> with 24 symmetrically equivalent variants is usually the only one. The case for hcp is more complicated because (0001)<1210> basal slip, {1010}<1210> prismatic slip, {1011}<1210> pyramidal <*a*>

Table 2. Slip Systems of fcc and hcp Metals As Used in the Simulations

Structure	Slip System	Slip Type	CRSS Ratio
fcc	{111}<110>		1
hcp	(0001)< $\bar{1}2\bar{1}0$>	basal slip	1
hcp	{$10\bar{1}0$}<$\bar{1}2\bar{1}0$>	prismatic slip	1
hcp	{$10\bar{1}1$}<$\bar{1}2\bar{1}0$>	pyramidal <a> slip	10
hcp	{$10\bar{1}1$}<$11\bar{2}3$>	pyramidal <c+a> slip	10

slip, {$10\bar{1}1$}<$11\bar{2}3$> pyramidal <*c*+*a*> slip and also several twinning modes have all been observed and influence texture development differently [*Lebensohn and Tomé,* 1993; *Lebensohn et al.,* 1996; *Tenckhoff,* 1974; 1978]. Hexagonal metals have been divided into two groups, those with a high *c/a* ratio such as Zn and Cd and others with a low c/a ratio such as Zr and Ti. Hexagonal ε-iron has a low *c/a* ratio, and therefore it has been suggested that it should behave similarly as titanium and zirconium with basal and prism <*a*> slip, respectively. There is uncertainty whether the *c/a* ratio or the stacking fault energy is more important in determining the exact values of critical shear stresses [*Poirier and Price,* 1999]. In any case in all hexagonal metals and particularly at high temperature more than one slip system become active (prismatic, basal, and pyramidal). The relative activity depends on grain orientation (Ti [*Pochettino et al.,* 1988; *Prantil et al.,* 1995], Be [*Greenspan,* 1965] Zr [*Akhtar,* 1973, 1975]). Critical resolved shear stress ratios for the systems used in our simulations are listed in Table 2. In hexagonal metals, mechanical twinning is not observed at high temperature, and pyramidal slip plays a secondary role. Consequently, basal and prismatic slip are the most likely active systems. With the fully anisotropic 1-site VPSC model it is possible to reproduce experimentally observed crystal orientation patterns of hexagonal metals, both at low and at high temperature conditions [*Lebensohn and Tomé,* 1994, 1996; *Lebensohn et al.,* 1996; *Tomé and Canova,* 1998].

We have explored the influence of relative ease of prismatic and basal slip on texture development by comparing simple shear simulations to strains of 50% and 100%. We assumed that prismatic slip is 2 times harder than basal slip (Figure 4, left side) and that basal slip is 2 times harder than prismatic slip (Figure 4, right side). The two patterns are very similar. Texture development is a bit stronger if basal slip is favored.

The reason for this can be easily figured out by analyzing the reorientation associated with both slip modes. While the plastic spin due to basal slip reorients the basal poles toward the most compressed direction, the one due to prismatic slip gives a rotation around the (0001) direction, leaving the basal pole orientation invariant. Provided the contribution of the local spin is negligible for equiaxed grains, the orientation distribution of the basal pole will be dictated by the superposition of the macro rotation and the plastic rotation associated with basal slip. Therefore, if basal slip is favored over prismatic slip, this would just speed up the alignment of the basal poles with the current compressive direction but would not qualitatively change the simulated basal texture pattern. In the core simulations we assumed that critical shear stresses for basal and prismatic slip were equal. This is consistent with direct observations of preferred orientation of ε-iron in diamond anvil experiments that suggest activity of basal slip [*Matthies et al.,* 1999]. We are satisfied that the uncertainty about exact critical shear stresses has little effect on final orientation of the basal poles and therefore on the predicted anisotropy of the seismic wave propagation velocities, contrary to the conclusions of *Poirier and Price* [1999].

A larger uncertainty than with slip system activity is associated with elastic constants (Table 3) which are needed to calculate elastic properties and seismic velocities of textured polycrystals by averaging. For ε-iron and γ-iron at core pressures these are based on first principles calculations at 0 K [*Stixrude and Cohen,* 1995; *Soderlind et al.,* 1996] and derived from polycrystal diamond anvil experiments at 54 GPa [*Singh et al.,* 1998] and 211 GPa [*Mao et al.,* 1998]. The

Table 3. Elastic Moduli for Selected Metals

	C_{11}	C_{33}	C_{44}	C_{12}	C_{13}	ρ	References
ε-Fe (hcp)	1801	1919	445	865	810	13	*Stixrude and Cohen* [1995] (core pressure)
ε-Fe (hcp)	2750	2780	767	893	1470	13	*Soderlind et al.* [1996] (400GPa, 0 K)
ε-Fe (hcp)	552	562	395	335	301		*Singh et al.* [1998] (52 GPa, Voigt)
ε-Fe (hcp)	639	648	422	300	254		*Singh et al.* [1998] (52 GPa, Hill)
ε-Fe (hcp)	1303	1302	960	637	637	13	*Mao et al.* [1998] (211 GPa)
γ-Fe (fcc)	1658	1658	636	941		13	*Stixrude and Cohen* [1995] (core pressure)
γ-Fe (fcc)	2208	2208	950	1536		13	*Soderlind et al.* [1996] (400 GPa, 0 K)
Ti (hcp)	160	181	46.5	90	66	4.5	*Brandes* [1983]
Zr (hcp)	144	166	33.4	74	67	6.5	*Brandes* [1983]
Zn (hcp)	163	63	39	36	53	7.1	*Brandes* [1983]

Stiffnesses in GPa and density in g/cm^3.

experimental data suggest a higher anisotropy for ε-iron. We will compare results for both.

4. Results

4.1. Texture Development

The convection pattern in an internally or bottom heated cell can be quite complex and time dependent (e.g., *Tackley,* 1996). In this exploratory study we have constrained the convection pattern to axial symmetry about the Earth's axis. This does not have a particular physical justification, except that it conforms to seismic observations. Calculations were done for harmonic degree one and harmonic degree two convection, and only results for harmonic degree two are shown. Going to higher orders would change details in the pattern and produce higher local heterogeneity.

A strongly time-dependent convection pattern is observed, dominated by degree two harmonic components. RMS velocities are of the order of 10 cm/yr; strain rates are of the order of 10^{-15} /s and stresses of the order of 10 Pa. The advective component of heat flux is 3 x 10^8 W, or about 0.1% of the conductive flux. Figure 1 shows three snapshots in time of the velocity field in the time-dependent solution. On the average there is no correlation between the orientation of the patterns with the coordinate axes. For convenience in our texture calculations we selected the pattern of the top snapshot in Figure 1 that does show good alignment with the coordinate axes and features downwelling flow at the coordinate poles and upwelling around the coordinate equator. A full cycle of the convection pattern takes about 50 million years.

Three streamlines from the pattern in Figures 1a and 1b are displayed in Figure 2 (only a quadrant of the shell is shown, with axial symmetry assumed along the N-S axis and a mirror plane in the equatorial plane). The external streamline displays a bulge around the central nucleus that was assumed to be rigid. As explained above, this nucleus was merely introduced for numerical stability and there is no visible effect on the flow pattern for the internal streamlines. One cycle for the outer trajectory (A) requires about 26 million years and for the inner cycle (C) requires 19 million years.

Texture simulations were performed for both fcc and hcp iron. Slip systems and critical shear stresses are listed in Table 2. As stress exponent we used 3 (in the finite element flow model a Newtonian fluid was assumed, n=1). An initial distribution of 400 randomly oriented grains was placed at points labeled "1" in Figure 2. It was assumed that no hardening takes place and that the grain shape remains equiaxed.

The strains arising from convection are large, with large changes, both for normal and shear components (particularly between points 2 and 4 of the external streamline (A) as illustrated in Figure 3), and texture development is intense. Figures 5 shows the evolution of texture for fcc, and Figure 6 shows the evolution of texture for hcp iron, both for the external (Figures 5a and 6a) and the intermediate trajectory (Figures 5b and 6b) for locations 1, 3, 5, and 7. We show (111) pole figures for fcc and (0001) pole figures for hcp. The poles to (111) and (0001) correspond to fast wave propagation directions in those crystals if elastic properties of *Stixrude and Cohen* [1995] are assumed. Keep in mind that these pole figures are not projections on the Earth but illustrate orientation distributions at different locations in the inner core. However, they are related to Earth coordinates in that the center is parallel to the N-S axis and the periphery parallel to the equatorial plane (contrary to Figure 2).

In the case of fcc (Figure 5) and an external trajectory, initially a strong extrusion texture forms (step

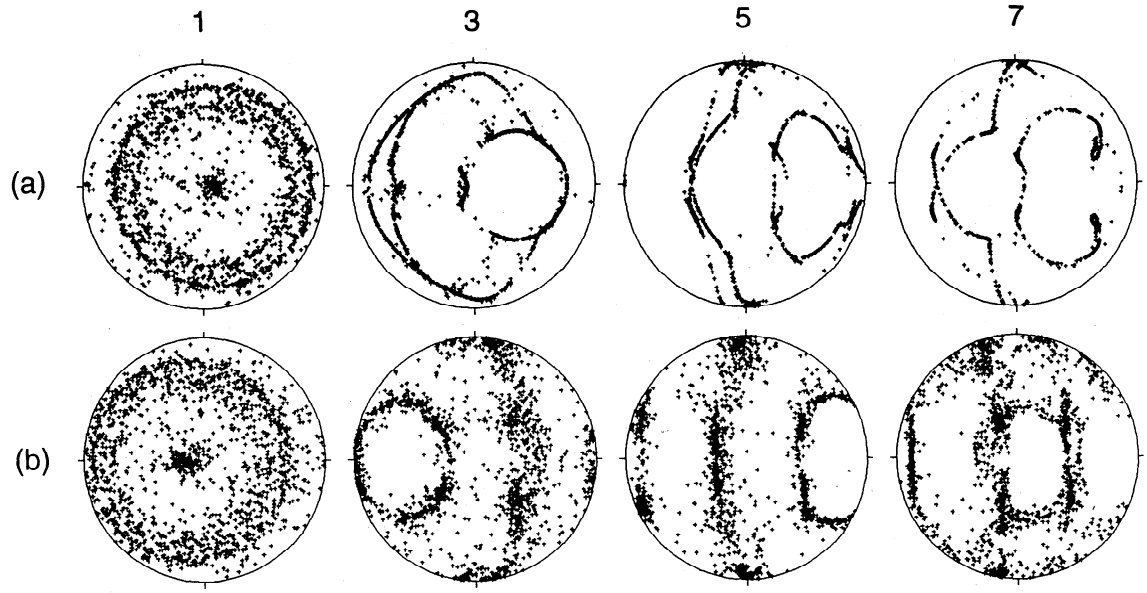

Figure 5. Texture development along the (a) external and (b) intermediate streamline for positions 1, 3, 5, and 7, as illustrated in Figure 2. It is assumed that the material is fcc iron deforming by (111)<110> slip; {111} pole figures for 400 grains are represented in equal-area projection. The N-S axis is at the center, and the equatorial plane is at the periphery.

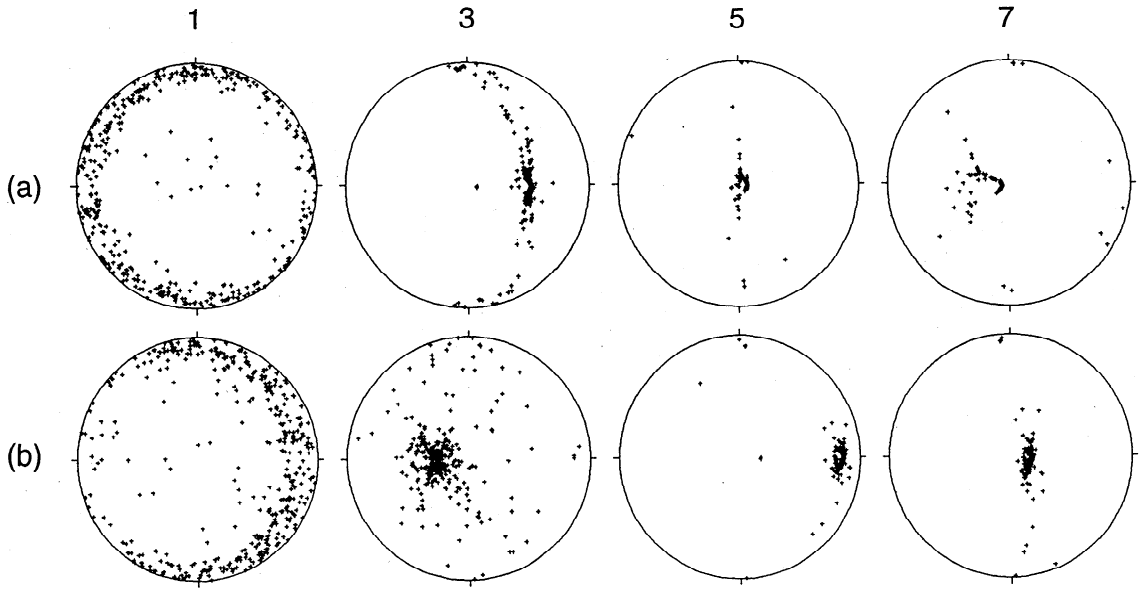

Figure 6. Texture development along the (a) external and (b) intermediate streamline for positions 1, 3, 5, and 7, as illustrated in Figure 2. It is assumed that the material is hcp iron deforming by basal and prismatic slip; 0001 pole figures (*c* axes) for 400 grains are represented in equal-area projection. The N-S axis is in the center and the equatorial plane is at the periphery.

1) with a typical (111) maximum in the extrusion direction and two small circles of (111) poles; (100) pole figures (not shown) also display a maximum in the extrusion direction. This is the typical double fiber texture observed during wire drawing of fcc metals [*Rollett and Wright,* 1998]. As the material gets drawn out into the equatorial plane, the texture becomes less symmetrical due to a shear component. As position 5 is approached, the main components of a rolling texture develop, without significant change between positions 5 and 7.

We are not showing textures along the outer part of the trajectory. In fact, texture patterns do not change greatly but simply undergo a rigid body rotation (Figure 3). In our texture simulations we have imposed that in the external region, close to the boundary with the liquid outer core, the texture reverts to random. A physical justification is that materials close to the melting point undergo annealing recrystallization, and texture strength is likely to be reduced. We impose that the texture remains random until the representative material volume reaches point 0 and then texture starts to develop again, as during the first cycle.

For the intermediate trajectory (B in Figure 2), texture development is less intense, again changing from an extrusion texture to a rolling texture. Overall, for fcc there is a (111) concentration in the polar direction. As we advance from position 5 to 8, the texture changes correspond mainly to a rigid body rotation as described above. In this case, the sequence of predicted textures do not change significantly after the first cycle.

If we assume that the material is hcp (Figure 6), texture patterns have the same symmetry as for fcc but are of course different. During subduction at the poles again an axisymmetric (fiber) texture develops, this time with *c* axes perpendicular to the N-S axis. As the material extrudes in the equatorial plane, this texture transforms to a strong (0001) maximum parallel to the N-S axis (positions 5), rotating as the material reaches the surface. For the internal trajectories, textures are again weaker but with a similar pattern. On the outer part of the external trajectory the texture changes are largely due to rigid body rotations. As illustrated above for simple shear (Figure 4), we have investigated the influence of relative critical shear stresses for basal and prismatic slip on texture development and observed that the effect on the *c* axis orientation distribution is minimal. Basal slip is mainly responsible for the texture evolution, even if it is a secondary slip system.

4.2. Seismic Velocity

The simulations indicate that during spherical convection strong textures develop. The patterns are rather complex and certainly very different from a single crystal. No immediate conclusions can be drawn about the overall anisotropy of elastic constants even though we expect higher velocities along concentrations of 111 poles for fcc iron and 0001 poles for hcp iron which are the fast single crystal directions. A more quantitative estimate is obtained by calculating aggregate elastic properties for locations along trajectories, based on single crystal properties and the orientation distribution.

Single crystals of hexagonal metals with a low *c/a* ratio, such as Ti and Zr, do not show a large anisotropy of elastic constants (Table 3). First principles calculations for ε-iron at core pressure support such a picture [*Stixrude and Cohen,* 1995; *Soderlind et al.,*

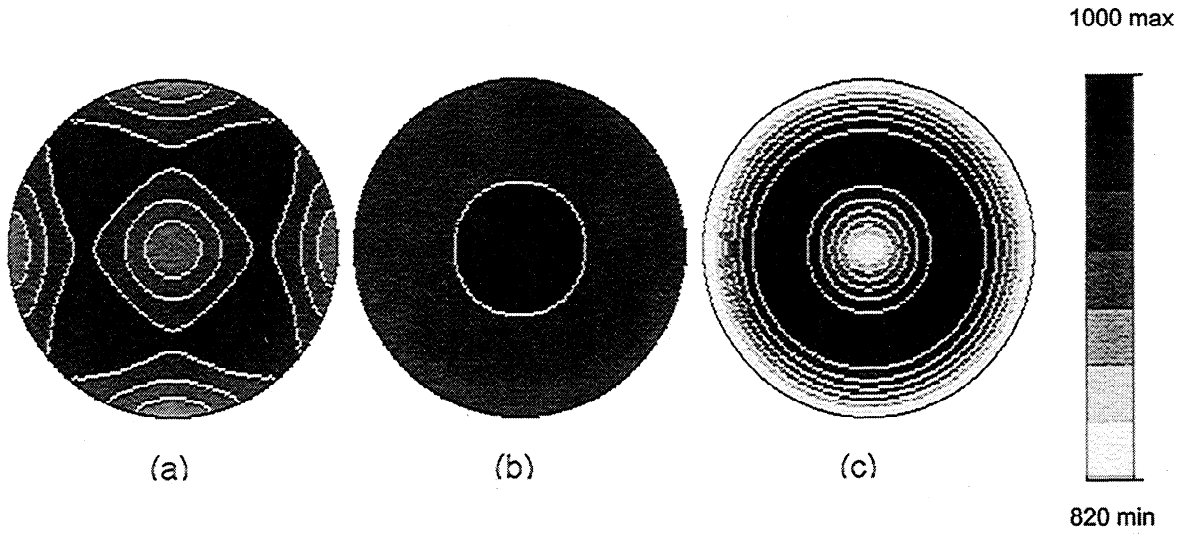

Figure 7. The P wave velocity surfaces for fcc (a) and hcp iron (b,c) single crystals at core pressure according to elastic properties from *Stixrude and Cohen* [1995] for Figures 7a and 7b and from *Mao et al.* [1998] for Figure 7c. The *c* axis is in the center; the surface is normalized so that the highest velocity is 1000 and the minimum is 825. A linear gray shade scale is indicated.

1996]. On the other hand recent experimental studies suggest that the anisotropy may be much larger [*Singh et al.,* 1998; *Mao et al.,* 1998]. In this study we investigated both cases.

Figure 7 shows equal-area projections of the *P* velocity surfaces for fcc and hcp single crystals normalized such that the maximum is 1000. The *c* axis is in the center of the figure. For fcc iron the highest velocity is near 111 and the minimum near 100. The anisotropy (difference between maximum and minimum velocity) is 10% (Figure 7a). For hexagonal crystals, elastic properties have axial symmetry, and therefore only the *c* axis is relevant. In the case of hcp iron and *Stixrude and Cohen*'s [1995] elastic constants, the highest velocity is close to the *c* axis with an anisotropy of 4% (Figure 7b). This is similar to titanium. For hcp iron and *Mao et al.* [1998] elastic constants, the maximum is on a ring about 40° from the *c* axis and the anisotropy is 18% (Figure 7c). This is similar to zinc.

If we know the crystal orientation and the elastic properties of the single crystal, then we can calculate elastic properties of the aggregate and the directional dependence of acoustic wave propagation by weighted averaging over the orientation distribution, for example,

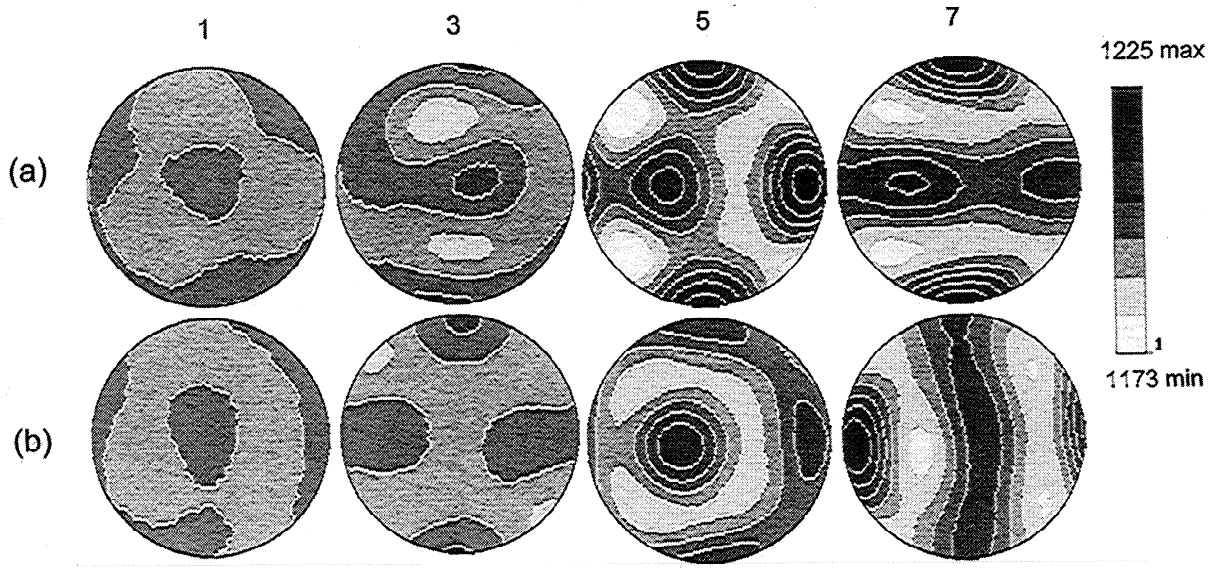

Figure 8. Polycrystal *P* wave velocity surfaces for fcc iron based on a self-consistent average of orientation distributions illustrated in Figure 5: (a) external (A) and (b) intermediate streamline (B) for positions 1, 3, 5, and 7, as illustrated in Figure 2.

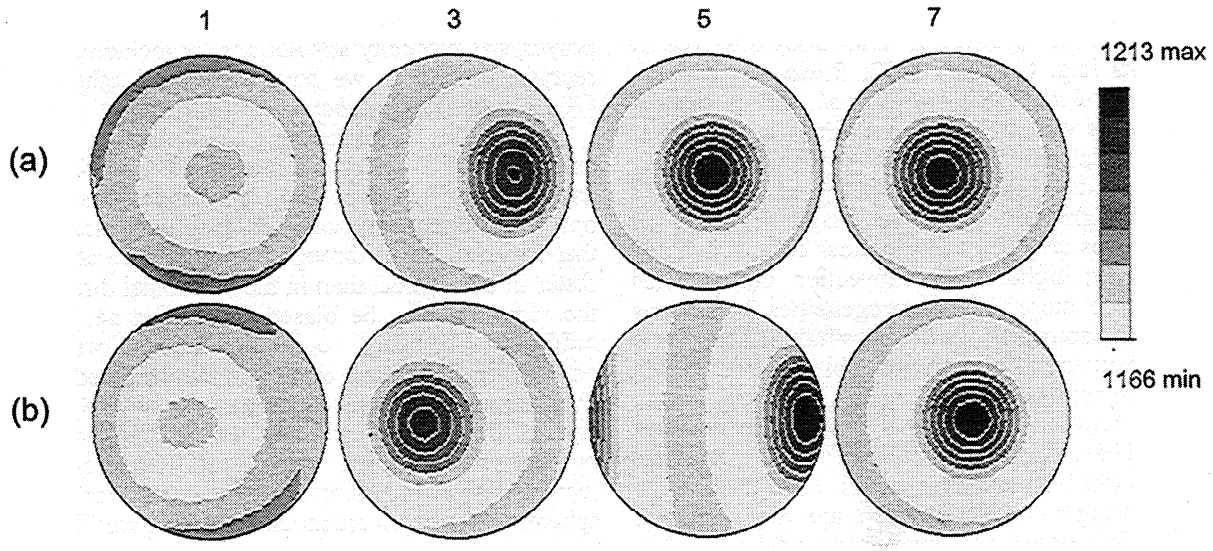

Figure 9. Polycrystal *P*-wave velocity surfaces for hcp iron based on a self-consistent average of orientation distributions illustrated in Figure 6 and elastic constants of *Stixrude and Cohen* [1995]: (a) external streamline (A) and (b) intermediate streamline (B) for positions 1, 3, 5, and 7, as illustrated in Figure 2.

with a self-consistent method [*Tomé,* 1998]. From polycrystal elastic properties we then calculated *P* wave velocity surfaces (assuming a density of 13 g/cm) and those are represented for the same positions (1-3-5-7) as pole figures (Figures 5 and 6) on (top) external and (bottom) intermediate trajectories for fcc (Figure 8) and hcp (Figures 9 and 10). Each of these velocity figures is representative for the particular location in the inner core sphere. The largest velocity difference is 4% for fcc, 4% for hcp [*Stixrude and Cohen,* 1995] and 17% for hcp [*Mao et al.,* 1998]. These anisotropies are close to those of single crystals. Overall high velocities are parallel to the N-S axis.

5. Discussion

FEM modeling of convection in a sphere and polycrystal plasticity simulations document large deformation and corresponding development of strong preferred orientation of crystals. Orientation patterns are variable within the convection cell according to the different strain gradients. Strain and corresponding textures are highest along an external streamline and weaker in the center of the convection cell. These general observations are true for harmonic degree one and two convection and would also apply to higher degree geometries. The lower degree geometries which

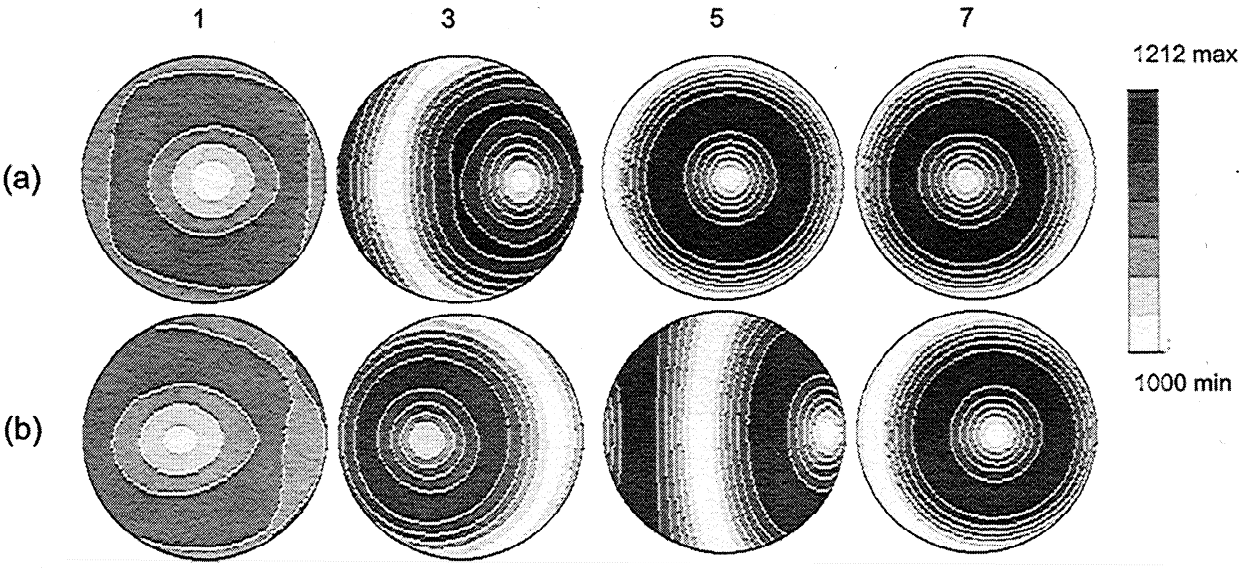

Figure 10. Polycrystal *P*-wave velocity surfaces for hcp iron based on a self-consistent average of orientation distributions illustrated in Figure 6 and elastic constants of *Mao et al.* [1998]: (a) external streamline (A) and (b) intermediate streamline (B) for positions 1, 3, 5, and 7, as illustrated in Figure 2.

we considered have axial symmetry and this agrees on first order with the "cylindrical" anisotropy observed by seismologists [e.g. *Creager,* 1992; *Romanowicz et al.,* 1996; *Shearer et al.,* 1988; *Vinnik et al.,* 1994]. Second-order harmonic was preferred over first- order because of the equatorial mirror plane that seemed more likely and corresponds with the symmetry of the Earth's rotation, though not with the magnetic field. If convection does take place in the inner core, it is likely that also some higher-order convection occurs. This would produce more local heterogeneities in patterns but overall anisotropies would be similar. This could explain recent detailed seismic observations which describe deviations from axial symmetry with differences between eastern and western hemispheres [*Creager,* 1999, *McSweeney et al.,* 1997; *Shearer,* 1994; *Song,* 1997; *Su and Dziewonski,* 1995].

Strains during a convection cycle are very high, and based on this a polycrystal plasticity model that relies solely on slip as deformation mechanism produces a very strong crystal alignment. If diffusion accompanies slip (e.g., during recovery), it is anticipated that the orientation pattern would be similar but with a wider spread of orientations. It has been illustrated by *Dawson and Wenk* [1999] that a more diffuse texture pattern has minimal effect on elastic properties because the elastic modulus is a lower-order property than texture.

At the high deformation and high temperature it is likely that deformation is accompanied by dynamic recrystallization. Recrystallization generally modifies the texture pattern. Depending on the system the strength of the texture may increase or decrease. If material is very close to the melting point and deformation gradients are weak (such as during spreading along the inner-outer core boundary), textures may be attenuated by random growth. In the context of this core model, that is a first-order survey, parameters are not sufficiently known (particularly the anisotropy distribution within the inner core) to warrant refining polycrystal plasticity simulations by including dynamic recrystallization as we have done with other systems [*Wenk et al.,* 1997; *Lebensohn et al.,* 1998].

With the convection simulations, maximum anisotropy of *P*-waves amounts to 10% for fcc and 4% and 17% for hcp depending on elastic constants. The only feature that seismologists have well established is that *P*-waves travel through the inner core about 3-4% faster in the vertical than in the horizontal direction, but the sampling may be biased [*Bréger et al.,* 1999]. In order to compare our simulations with those observations, we have done volume-weighted averages over the whole sphere. Since we only have 8 points on each of the three streamlines, we perform this average by assigning to each step along the streamlines a representative volume. In these averages over the whole sphere, anisotropies are much lower (Figure 11). For fcc and hcp iron [*Stixrude and Cohen,* 1995] the highest velocities are still parallel to the N-S axis but anisotropies are only 0.5% and 2%, respectively. For hcp [*Mao et al.,* 1998], highest velocities are on a ring at 40° to the N-S axis and the anisotropy is 5%. We are aware that such a bulk average over a large volume with heterogeneous anisotropy is only a first-order approximation of expected seismic effects. For a more detailed description wave propagation through a heterogeneous anisotropic medium would have to be considered.

Our study documents that deformation during inner core convection would produce crystal alignments that could cause elastic anisotropy consistent with presently available seismic observations. We also have made a case that physical properties and conditions in the inner core may be conducive for convection. We can not exclude that processes other than convection may produce seismic anisotropy. In our view, melt-textured growth would rather produce a radial texture than a

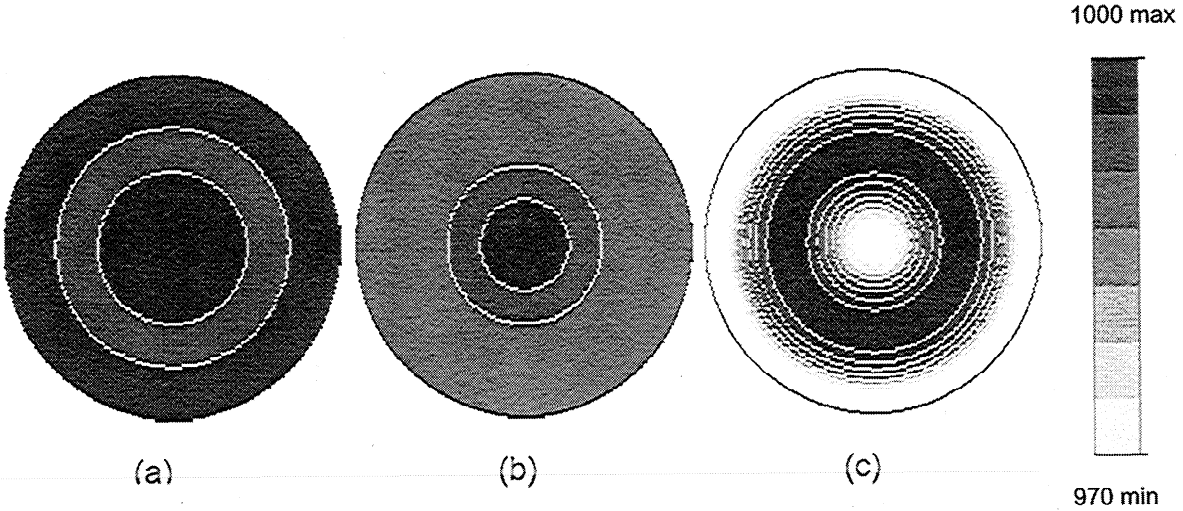

Figure 11. Volume-weighted average of elastic properties over the whole inner core and corresponding *P* wave velocity surfaces. Pole is in the center and equator at the periphery. Linear scale with gray shades is indicated. Maximum is 1000 and minimum 955. Average for (a) fcc iron, (b) hcp iron [*Stixrude and Cohen,* 1995], and (c) hcp iron [*Mao et al.,* 1998], corresponding to the polycrystal plasticity simulations in Figures 5 and 6. It is assumed that the outermost shell has a random orientation distribution.

single crystal, with little overall anisotropy. And particularly, a single crystal of huge dimensions and spherical shape appears very unlikely, since growth velocities of hexagonal metals are very anisotropic. In view of the high Rayleigh numbers it would appear that even if a single crystal or a highly aligned polycrystal would grow in a melt it would, in the course of the Earth's history, be subject to deformation and recrystallize. While growth as proposed, for example, by *Karato* [1993] or *Yoshida et al.* [1996] produces a static ("frozen") anisotropy, texture development during convection (whether it is solely by slip or accompanied by dynamic recrystallization) is a dynamic process and changes. The finite element calculations suggest that a convection cycle may take 10-20 million years and that the convective flow itself may cycle through different patterns over 40-60 million years. Note that these dynamics are not related to the temporal changes in inner core anisotropy recently observed and attributed to a rigid body rotation of the inner core relative to the mantle on a much shorter timescale of a few hundred years [*Song and Richards,* 1996].

The notion that growth of crystals in the inner core is caused by stresses imposed by convection of the outer core [*Yoshida et al.*, 1996] is also subject to the assumption that convection does not occur inside the inner core. It is well-established in metals that growth (grain boundary migration) is controlled by the deformation state of a crystal, rather than an imposed stress as suggested by the *Kamb* [1959] model. This model, which relies on thermodynamics, has only been applicable to situations such as "pressure solution", but not dynamic recrystallization. Energies introduced by dislocations are orders of magnitudes higher than disequilibrium due to stress. But it is conceivable that a magnetic field could modify growth selection during dynamic recrystallization [*Karato,* 1993]. Also the magnetic field and resulting Maxwell stress could be the cause of ductile flow in the inner core [*Karato,* 1999], rather than thermally driven convection. Such concepts could be included in a refined version of the convection model.

A test to distinguish between convection-produced deformation texturing and preferential growth could come from a more detailed tomographic study of inner core structure. Investigations such as those of *Su and Dziewonski* [1995] go in that direction. Originally it was postulated that anisotropy is concentrated in the outermost 300 km of the inner core [*Tromp,* 1993]. But this opinion has been reversed [*Song,* 1996; *Song and Helmberger,* 1995] to the point of suggesting that anisotropy extends throughout the inner core and that in fact the outer 100 km may not be anisotropic at all, consistent with our model of random growth close to the inner-outer core boundary. Convection models would predict large local variations and different velocities for waves passing through the core, either horizontally or vertically, in the equatorial plane and at medium latitudes.

A distinguishing difference then between a dynamic convection-deformation mechanism and a static growth concept is the character of the anisotropy each produces, whether it is heterogeneous or homogeneous. This puts the burden on seismologists who have, as a first step, to confirm if anisotropy in the inner core is real or an artifact [*Bréger et al.,* 1999] and, if anisotropy prevails, to detail the directionality and local distribution. If heterogeneity suggests that convection is active, the model presented here can be refined and generalized to attempt to account for such data. In particular, one could more confidently decide between a fcc and hcp (or other) structure for the inner core mineralogy. We could also explore the anisotropy due to changing patterns produced by the time-dependent convective flow. At this point it would become reasonable to include mechanisms such as recrystallization and the influence of the magnetic field.

In conclusion, we have shown that if there is sufficient internal heating in the inner core, convection occurs and produces strong deformation. This leads to crystal preferred orientation and elastic anisotropy.

Acknowledgments. We are grateful for discussions with colleagues, among them L. Bréger, M. Bukowinski, S. Karato, B. Romanowicz, and D. Stevenson and comments by reviewers. Particularly D. Stevenson made us aware of the limiting conditions for convection. The work was supported by IGPP-LANL (Proposal 603) and NSF (grant EAR 99-02866).

References

Akhtar, A., Basal slip in zirconium, *Acta Metall., 21*, 1-11, 1973.

Akhtar, A., Prismatic slip in zirconium single crystals at elevated temperatures, *Metall. Trans. A, 6,* 1217-1222, 1975.

Anderson, D.L., Bulk attenuation in the Earth and viscosity of the core, *Nature, 285,* 204-207, 1980.

Anderson, O.L., The high-pressure triple points of iron and their effects on the heat flow from the Earth's core, *J. Geophys. Res. 95,* 21,697-21,707, 1990.

Anderson, W.W., and T.J. Ahrens, Shock temperature and melting in iron sulfides at core pressures, *J. Geophys. Res., 101,* 5627-5642, 1996.

Baumgardner, J.R., Application of supercomputers to 3-D mantle convection, in *The Physics of the Planets*, edited by S. K. Runcorn, pp. 199-231, John Wiley, New York, 1988.

Baumgardner, J.R., Three-dimensional treatment of convective flow in the Earth's mantle, *J. Stat. Phys., 39,* 501-511, 1985.

Bergman, M.I., Measurements of elastic anisotropy due to solidification texturing and the implications for the Earth's inner core, *Nature, 389,* 60-63, 1997.

Boehler, R., Temperatures in the Earth's core from melting point measurements of iron at high static pressures, *Nature, 363,* 534-536, 1993.

Brandes, E.A., *Smithell's Metals Reference Book*, Butterworths, London, 1983.

Bréger, L., B. Romanowicz, and H. Tkalcic, PKP(BC-DF) travel time residuals and short scale heterogeneity in the deep earth, *Geophys. Res. Lett., 26,* 3169-3172, 1999.

Brown, J.M., and R.G. McQueen, Phase transitions, Gruneisen parameter, and elasticity for shocked iron between 77 Gpa and 400 Gpa, *J. Geophys. Res., 91*, 7485-7494, 1986.

Buffett, B.A., and K.C. Creager, Rotation and deformation of the inner core, *Eos Trans. AGU, 79* (17) Spring Meet. Suppl., S218-S219, 1998.

Bukowinski, M.S.T., The effect of pressure on the physics and chemistry of potassium, *Geophys. Res. Lett., 3,* 491-494, 1976.

Bukowinski, M.S.T., Compressed potassium: A siderophile element, in *High Pressure Science and Technology*, edited by K.D. Timmerhaus and M.S. Barber, pp. 237-244, Plenum, New York, 1979.

Canova, G.R., H.-R. Wenk, and A. Molinari, Simulation of texture development in polyphase materials, *Acta Metall. Mater., 40,* 1519-1530, 1992.

Chandrasekhar, S., *Hydrodynamic and Hydromagnetic Stability*, Dover, Mineola, N. Y., 1961.

Chastel, Y.B., P.R. Dawson, H.-R. Wenk, and K. Bennett, Anisotropic convection with implications for the upper mantle, *J. Geophys. Res., 98,* 17,757-17,771, 1993.

Crampin, S., A review of wave motion in anisotropic and cracked elastic media, *Wave Motion, 3,* 242-391, 1981.

Creager, K.C., Anisotropy of the inner core from differential travel times of the phases PKP and PKIKP, *Nature, 356,* 309-314, 1992.

Creager, K.C., Large-scale variations in inner core anisotropy, *J. Geophys. Res., 104,* 23,127-23,139, 1999.

Dawson, P.R., and H.-R. Wenk, Anisotropy development in the upper mantle based on polycrystal plasticity, *Philos. Mag. A.*, in press, 1999.

DeRango, P., M. Lees, P. Lejay, A. Sulpice, R. Tournier, M. Ingold, P. Germi, and P. Pernet, Texturing of magnetic materials at high temperature by solidification in a magnetic field, *Nature, 349,* 770-772, 1991.

Doherty, R.D., Recrystallization and texture, *Prog. Mater. Sci., 42,* 39-58, 1997.

Dziewonski, A.M., and D.L. Anderson, Preliminary reference Earth model, *Phys. Earth Planet. Inter. 25,* 297-356, 1981.

Frost, H.J., and M.F. Ashby, *Deformation Mechanism Maps*, Pergamon, Tarrytown, N.Y., 1982.

Glatzmaier, G.A., and P.H. Roberts, A three-dimensional self-consistent computer simulation of a geomagnetic field reversal, *Nature, 377,* 203-209, 1995.

Glatzmaier, G.A., and P.H. Roberts, An anelastic evolutionary geodynamo simulation driven by compositional and thermal convection, *Physica D, 97,* 81-94, 1996.

Greenspan, J., Ductility problems, in *Beryllium, Its Metallurgy and Properties*, edited by H.H. Hausner, pp. 240-246, Univ. of Calif. Press, Berkeley, 1965.

Haessner, F., *Recrystallization of Metallic Materials*, Riederer, Stuttgart, 1978.

Huang, S.C., R.P. Laforce, A.M. Ritter, and R.P. Goehner, Rapid solidification characteristics in melt spinning a Ni-base superalloy, *Metall. Trans. A, 16,* 1773-1779, 1985.

Humphreys, F.J., and M. Hatherly, *Recrystallization and Related Annealing Phenomena*, Oxford Univ. Press, New York, 1995.

Jeanloz, R., The nature of the Earth's core, *Annu. Rev. Earth Planet. Sci., 18,* 357-386, 1990.

Jeanloz, R., and H.-R. Wenk, Convection and anisotropy of the inner core, *Geophys. Res. Lett., 15,* 72-75, 1988.

Jephcoat, A., and P. Olson, Is the inner core of the Earth pure iron?, *Nature, 325,* 332-335, 1987.

Jephcoat, A.P., H.K. Mao, and P.M. Bell, Static compression of iron to 78 Gpa with rare gas solids as pressure-transmitting media, *J. Geophys. Res., 91,* 4677-4684, 1986.

Kamb, W.B., Theory of preferred crystal orientation developed by crystallization under stress, *J. Geol.*, 67, 153-170, 1959.

Karato, S., Inner core anisotropy due to magnetic field-induced preferred orientation of iron, *Science, 262,* 1708-1711, 1993.

Karato, S., Seismic anisotropy of the Earth's inner core caused by the Maxwell stress-induced flow, *Nature,* in press, 1999.

Kocks, U.F., C.N. Tomé, and H.-R. Wenk, *Preferred Orientations in Polycrystals and Their Effect on Materials Properties*, Cambridge Univ. Press, Cambridge, U.K., 1998.

Lebensohn, R.A., and C.N. Tomé, A self-consistent anisotropic approach for the simulation of plastic deformation and texture development of polycrystals: Application to zirconium alloys, *Acta Metall. Mater., 41,* 2611-2624, 1993.

Lebensohn, R.A., and C.N. Tomé, A self-consistent visco-plastic model: prediction of rolling textures of anisotropic polycrystals, *Mater. Sci. Eng. A, 175,* 71-82, 1994.

Lebensohn, R.A., and C.N. Tomé, Yield loci calculation of hexagonal materials using a self-consistent polycristalline model, *Textures Microstructures, 26-27,* 513-529, 1996.

Lebensohn, R.A., M.I. Gonzales, C.N. Tomé and A.A. Pochettino, Measurement and prediction of texture development during a rolling sequence of zircaloy-4 tubes, *J. Nucl. Mater., 229,* 57-64, 1996.

Lebensohn, R.A., H.-R. Wenk, and C. Tomé, Modelling deformation and recrystallization textures in calcite, *Acta Mater., 46,* 2683-2693, 1998.

Mao, H.K., Y. Wu, L.C Chen, and J.F.Shu, Static compression of iron to 300 Gpa and Fe0.8Ni0.2 alloy to 260 Gpa: Implications for composition of the core, *J. Geophys. Res., 95,* 21,737-21,742, 1990.

Mao, H.K., J. Shu, G. Shen, R.J. Hemley, B. Li, and A.K. Singh, Elasticity and rheology of iron above 220 GPa and the nature of the Earth's inner core, *Nature, 396,* 741-743, 1998.

Masters, T.G. and P.M. Shearer, Summary of seismological constraints on the structure of the Earth's core, *J. Geophys. Res., 95,* 21,691-21,695, 1990.

Matthies, S., H.-R. Wenk, H.K. Mao, and, R.J. Hemley, Preferred orientation of ε-iron produced in diamond anvil cells: Implications for deformation in the inner core (abstract), *Eos Trans. AGU, 80* (46), F21, Fall Meet. Suppl., 1999.

McSweeney, T.J., K,C, Creager, and R.T. Merrill, Depth extent of inner-core seismic anisotropy and implications for geomagnetism, *Phys. Earth Planet. Inter., 101,* 131-156, 1997.

Merrill, R.T., and M.W. McElhinny, *The Earth's Magnetic Field*, Academic, San Diego, Calif., 1983.

Molinari, A., G.R. Canova, and S. Ahzi, A self-consistent approach of the large deformation polycrystal viscoplasticity, *Acta Metall., 35,* 2983-2994, 1987.

Morelli, A., A.M. Dziewonski, and J.H.Woodhouse, Anisotropy of the core inferred from PKIKP travel times, *Geophys. Res. Lett., 13,* 1545-1548, 1986.

Parker, L. J., T. Atou, and J. V. Badding, Transition element-like chemistry for potassium under pressure, *Science, 273,* 95-97, 1996.

Pochettino, A., C. Tomé, P. Vedoya, and R. Penelle, Analysis of plastic anisotropy in titanium sheets - microstructural considerations, in *Proc. Sixth World Conference on Titanium, Cannes, France*, edited by P. Lacombe, pp 129-134, Les Editions de Physique, Paris, 1988.

Poirier, J.-P., and G.D. Price, Primary slip system of ε-iron and anisotropy of the Earth's inner core, *Phys. Earth Planet. Inter., 110,* 147-156, 1999.

Prantil, V.C., J.T. Jenkins, and P.R. Dawson, Modeling deformation induced textures in titanium using analytical solutions for constrained single crystal response, *J. Mech. Phys. Solids, 43,* 1283-1302, 1995.

Rollett, A.D., and S.I.Wright, Typical textures in metals, in *Texture and Anisotropy. Preferred Orientations in Polycrystals and Their Effect on Materials Properties,* edited by U.F. Kocks, C. Tome and H.-R. Wenk, pp. 178-238, Cambridge Univ. Press, Cambridge, U.K., 1998.

Romanowicz, B., X.D. Li and J. Durek, Anisotropy of the inner core: Could it be due to low-order convection?, *Science, 274,* 963-966, 1996.

Ross, M., D.A. Young, and R. Grover, Theory of the iron phase diagram at Earth core conditions, *J. Geophys. Res., 95,* 21,713-21,716, 1990.

Sachs, G., Zur Ableitung einer Fliessbedingung, *Z. Ver. Dtsch. Ing., 72,* 734-736, 1928.

Saxena, S., G. Shen, and P. Lazor, Experimental evidence for a new iron phase and implications for Earth's core, *Science, 260,* 1312-1314, 1993.

Sayers, C.M., The crystal structure of iron in the Earth's inner core, *Geophys. J. Int., 103,* 285-286, 1990.

Selvanickam, V., and K. Salama, Anisotropy and intergrain current density in oriented grained bulk Yba2Cu3Ox superconductor, *Appl. Phys. Lett., 57,* 1575-1577, 1990.

Shearer, P.M., Constraints on inner core anisotropy from PKP(DF) travel times, *J. Geophys. Res., 99,* 19,647-19,659, 1994.

Shearer, P.M., K.M. Toy, and J.A. Orcutt, Axisymmetric Earth models and inner core anisotropy, *Nature, 333,* 228-232, 1988.

Singh, D.J., W.E. Pickett, and H. Krakauer, Gradient-corrected density functionals: Full-potential calculations for iron, *Phys. Rev. B, 43,* 11,628-11,634, 1991.

Singh, A.K., H.-K. Mao, J. Shu, and R.J.Hemley, Estimation of single-crystal elastic moduli from polycrystalline x-ray diffraction at high pressure: Application to FeO and iron, *Phys. Rev. Lett., 80,* 2157-2160, 1998.

Soderlind, P., J.A. Moriarty, and J.M. Wills, First principles theory of iron up to earth-core pressures: Structural, vibrational, and elastic properties, *Phys. Rev. B, 53,* 14,063-14,072, 1996.

Song, D., and P.G. Richards, Observational evidence for differential rotation of the Earth's inner core, *Nature, 382,* 221-224, 1996.

Song, X., Anisotropy in central part of inner core. *J. Geophys. Res., 101,* 16,089-16,097, 1996.

Song, X., Anisotropy of the Earth's inner core, *Rev. Geophys., 35,* 297-313, 1997.

Song, X., and D.V. Helmberger, Depth dependence of anisotropy in Earth's inner core, *J. Geophys. Res., 100,* 9805-9816, 1995.

Stacey, F.D., *Physics of the Earth*, Brookfield, Auckland, New Zealand, 1992.

Stevenson, D.J., Models of the Earth's core, *Science, 214,* 611-619, 1981.

Stixrude, L., and J.M. Brown, The Earth's core, in *Ultrahigh-Pressure Mineralogy: Physics and Chemistry of the Earth's Deep Interior,* edited by R.J. Hemley, *Rev. Mineral., 37,* 261-282, 1998.

Stixrude, L., and R.E. Cohen, High-pressure elasticity of iron and anisotropy of Earth's inner core, *Science, 267,* 1972-1975, 1995.

Su, W.-J., and A.M.Dziewonski, Inner core anisotropy in three dimensions, *J. Geophys. Res., 100,* 9831-9852, 1995.

Tackley, P.J., Effects of strongly variable viscosity on three-dimensional compressional convection in planetary mantles, *J. Geophys. Res., 101,* 3311-3332, 1996.

Taylor, G.I., Plastic strain in metals, *J. Inst. Met., 62*, 307-324, 1938.

Tenckhoff, E., Operable deformation systems and mechanical behavior of textured zircaloy tubing, in *Zirconium in Nuclear Applications, ASTM STP 551*, 179-200, 1974.

Tenckhoff, E., The development of the deformation texture in zirconium during rolling in sequential passes, *Metall. Trans. A, 9,* 1401-1412, 1978.

Tomé, C.N., Tensor properties of textured polycrystals, in *Texture and Anisotropy. Preferred Orientations in Polycrystals and Their Effect on Materials Properties,* edited by U.F. Kocks, C. Tomé and H.-R. Wenk, pp. 282-324, Cambridge Univ. Press, Cambridge, U.K., 1998.

Tomé, C.N., and G.R. Canova, Self-consistent modeling of heterogeneous plasticity, in *Texture and Anisotropy. Preferred Orientations in Polycrystals and Their Effect on Materials Properties,* edited by U.F. Kocks, C. Tomé and H.-R. Wenk, pp. 466-510, Cambridge Univ. Press, Cambridge, U.K., 1998.

Tromp, J., Support for anisotropy of the Earth's inner core from free oscillations, *Nature, 366,* 678-681, 1993.

Vinnik, L., B. Romanowicz and L. Bréger, Anisotropy in the center of the inner core, *Geophys. Res. Lett., 21,* 1671-1674, 1994.

Wasserman, E., L. Stixrude, and R.E. Cohen, Thermal properties of close-packed phases of iron at high pressures and temperatures, *Phys. Rev. B, 53,* 8296-8309, 1996.

Wenk, H.-R., A voyage through the deformed Earth with the self-consistent model, *Model. Simul. Mater. Sci. Engin., 7,* 699-722, 1999.

Wenk, H.-R., and C.N. Tomé, Modeling dynamic recrystallization of olivine deformed in simple shear, *J. Geophys. Res., 104,* 25,513-25,527, 1999.

Wenk, H.-R., T. Takeshita, R. Jeanloz and G.C. Johnson, Development of texture and elastic anisotropy during deformation of hcp metals, *Geophys. Res. Lett., 15,* 76-79, 1988.

Wenk, H.-R., G. Canova, Y. Brechet, and L. Flandin, A deformation-based model for recrystallization, *Acta Mater., 45,* 3283-3296, 1997.

Wenk, H.-R., S. Matthies, J. Donovan, and D. Chateigner, BEARTEX, a Windows-based program system for quantitative texture analysis. *J. Appl. Cryst., 31,* 262-269, 1998.

Williams, Q.R., R. Jeanloz, J. Bass, B. Svendsen, and T.J. Ahrens, The melting curve of iron to 250 gigapascals: A constraint on the temperature at Earth's center, *Science, 236,* 181-182, 1987.

Woodhouse, J.H., D. Giardini, and X.D. Li, Evidence for inner core anisotropy from free oscillations, *Geophys. Res. Lett., 13,* 1549-1552, 1986.

Yoo, C.S., J. Akella, A.J. Campbell, and H.K. Mao, Phase diagram of iron by in situ x-ray diffraction: implications for Earth's core, *Science, 270,* 1473-1475, 1995.

Yoshida, S., I. Sumita, and M. Kumazawa, Growth model of the inner core coupled with the outer core dynamics and the resulting elastic anisotropy, *J. Geophys. Res., 101,* 28,085-28,103, 1996.

Zebib, A., G. Schubert, J.L. Dein, and R.C. Paliwal, Character and stability of axisymmetric thermal convection in spheres and spherical shells, *Geophys. Astrophys. Fluid Dyn., 23,* 1-42, 1983.

J.R. Baumgardner, Theoretical Division, MS B216, Los Alamos National Laboratory, Los Alamos, NM 87545. (baumgardner@lanl.gov)

R.A. Lebensohn, CONICET, University of Rosario, Av. 27 de Febrero 217BIS, 2000 Rosario, Argentina. (ricardo@ifir.ifir.edu.ar)

C. N. Tomé, Materials Science and Technology Division, MST-8, MS G755, LANL, Los Alamos NM 87545. (tome@lanl.gov)

H.-R. Wenk Department of Geology and Geophysics, University of California, Berkeley CA 94720. (wenk@seismo.berkeley.edu)

(Received January 20, 1999; revised September 1, 1999; accepted September 24, 1999.)